J|A|C|S
ARTICLES
Published on Web 03/31/2007

Proton-Directed Redox Control of O−O Bond Activation by Heme Hydroperoxidase Models

Jake D. Soper,[†] Sergey V. Kryatov,[‡] Elena V. Rybak-Akimova,[‡] and Daniel G. Nocera*,[†]

Contribution from the Department of Chemistry, 6-335, Massachusetts Institute of Technology, 77 Massachusetts Avenue, Cambridge Massachusetts 02139-4207, and Department of Chemistry, Tufts University, 62 Talbot Avenue, Medford, Massachusetts 02155

Received November 20, 2006; E-mail: nocera@mit.edu

Abstract: Hangman metalloporphyrin complexes poise an acid−base group over a redox-active metal center and in doing so allow the "pull" effect of the secondary coordination environment of the heme cofactor of hydroperoxidase enzymes to be modeled. Stopped-flow investigations have been performed to decipher the influence of a proton-donor group on O−O bond activation. Low-temperature reactions of tetramesitylporphyrin (TMP) and Hangman iron complexes containing acid (HPX−CO_2H) and methyl ester (HPX−CO_2Me) functional groups with peroxyacids generate high-valent Fe=O active sites. Reactions of peroxyacids with (TMP)Fe^{III}(OH) and methyl ester Hangman (HPX−CO_2Me)Fe^{III}(OH) give both O−O heterolysis and homolysis products, Compound I (Cpd I) and Compound II (Cpd II), respectively. However, only the former is observed when the hanging group is the acid, (HPX−CO_2H)Fe^{III}(OH), because odd-electron homolytic O−O bond cleavage is inhibited. This proton-controlled, $2e^-$ (heterolysis) vs $1e^-$ (homolysis) redox specificity sheds light on the exceptional catalytic performance of the Hangman metalloporphyrin complexes and provides tangible benchmarks for using proton-coupled multielectron reactions to catalyze O−O bond-breaking and bond-making reactions.

Introduction

Heme hydroperoxidase enzymes are divided into subclasses of peroxidases, catalases, and cytochrome P450 monooxygenases.[1] These enzymes are responsible for a wide array of biological redox processes, which originate from an Fe^{III} active site with protoporphyrin IX prosthetic groups.[2] Peroxidase enzymes are important for plant cell wall biosynthesis and lignin formation,[3] removal of xenobiotics, and signaling during oxidative stress.[4] Catalases work to eliminate cytotoxic hydrogen peroxide in vivo while avoiding the formation of harmful hydroxyl radical species,[5] and cytochrome P450 is responsible for a variety of metabolic oxidation reactions.[6,7] The diversity of biological redox processes performed by these enzymes is apparently achieved via a remarkably similar active oxidant, commonly called Compound I (Cpd I).[2,8−11] Cpd I is two redox levels above Fe^{III} with a ferryl Fe^{IV}=O and associated radical (e.g., a porphyrin π-radical cation, $P^{\bullet+}$, in horseradish peroxidase [HRP] and catalase, or an oxidized tryptophan in cytochrome *c* peroxidase [C*c*P]).[9−10,12] It is generated by heterolysis of an O−O bond in H_2O_2 or O_2. Such heterolytic cleavage to release H_2O is accomplished by an internal redox disproportionation coupled to the delivery of a H^+, from a precisely positioned acid/base residue in the active-site cavity to the distal O-atom in an Fe^{III}−OOH complex.[1,2,4,8−10,13−16] In peroxidases such as HRP, it is generally accepted that two residues in the distal cavity of HRP (His42 and Arg38) assist this reaction by shuttling protons to facilitate H_2O release (see Scheme 1).[16−20] Experi-

[†] Massachusetts Institute of Technology.
[‡] Tufts University.

(1) Suslick, K. S. In *The Porphyrin Handbook*; Kadish, K. M., Smith, K. M., Guilard, R., Eds.; Academic Press: San Diego, 2000; Vol. 4, pp 41−63.
(2) *Cytochrome P-450 Structure, Mechanism and Biochemistry*; Ortiz de Montellano, P. R., Ed.; Plenum Press: New York, 1986.
(3) Poulos, T. L.; Fenna, R. E. In *Metal Ions in Biological Systems*; Sigel, H., Sigel, A., Eds.; Dekker: New York, 1994; Vol. 30, pp 25−75.
(4) Rodriguez-Lopez, J. N.; Lowe, D. J.; Hernandez-Ruiz, J.; Hiner, A. N. P.; Garcia-Canovas, F.; Thorneley, R. N. F. *J. Am. Chem. Soc.* **2001**, *123*, 11838−11847.
(5) Meunier, B. In *Biomimetic Oxidations Catalyzed by Transition Metal Complexes*; Meunier, B., Ed.; Imperial College: London, 2000; pp 171−214.
(6) Sono, M.; Roach, M. P.; Coulter, E. D.; Dawson, J. H. *Chem. Rev.* **1996**, *96*, 2841−2887.
(7) Ortiz de Montellano, P. R. *Cytochrome P450: Structure Mechanism, and Biochemistry*, 2nd ed.; Plenum: New York, 1995.
(8) Sono, M.; Roach, M. P.; Coulter, E. D.; Dawson, J. H. *Chem. Rev.* **1996**, *96*, 2841−2887.
(9) Dunford, H. B. *Heme Peroxidases*; Wiley: New York, 1999.
(10) Watanabe, Y. In *The Porphyrin Handbook*; Kadish, K. M., Smith, K. M., Guilard, R., Eds.; Academic Press: San Diego, 2000; Vol. 4, pp 97−117.
(11) Newcomb, M.; Zhang, R., Chandrasena, R. E. P.; Halgrimson, J. A.; Horner, J. H.; Makris, T. M.; Sligar, S. G. *J. Am. Chem. Soc.* **2006**, *128*, 4580−4581.
(12) Sivaraja, M.; Goodin, D. B.; Smith, M.; Hoffman, B. M. *Science* **1989**, *245*, 738−740.
(13) Veitch, N. C.; Smith, A. T. *Advances in Inorganic Chemistry*; Academic Press: New York, 2001; Vol. 51, pp 107−162.
(14) Newcomb, M.; Chandrasena, R. E. P. *Biochem. Biophys. Res. Commun.* **2005**, *338*, 394−403.
(15) Davydov, R.; Chemerisov, S.; Werst, D. E.; Rajh, T.; Matsui, T.; Ikeda-Saito, M.; Hoffman, B. M. *J. Am. Chem. Soc.* **2004**, *126*, 15960−15961.
(16) Hiner, A. N. P.; Raven, E. L.; Thorneley, R. N. F.; Garcia-Canovas, F.; Rodriguez-Lopez, J. N. *J. Inorg. Biochem.* **2002**, *91*, 27−34.
(17) Ozaki, S.-I.; Roach, M. P.; Matsui, T.; Watanabe, Y. *Acc. Chem. Res.* **2001**, *34*, 818−825.
(18) Poulos, T. L.; Kraut, J. *J. Biol. Chem.* **1980**, *255*, 8199−8205.
(19) Matsui, T.; Ozaki, S-I.; Liong, E.; Phillips, G. N.; Watanabe, Y. *J. Biol. Chem.* **1999**, *274*, 2838−2844.
(20) Derat, E.; Shaik, S. *J. Phys. Chem. B* **2006**, *110*, 10526−10533.

Scheme 1

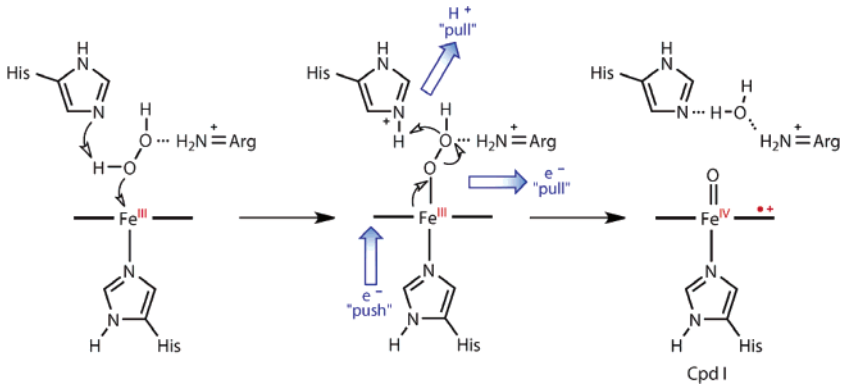

mental and computational studies support the hypothesis that His42 likely acts first as a base and then an acid.[4,17,20] In this way, the histidine does the "pull" part of the "push−pull mechanism" for peroxide activation.[8,10,13,21,22] The "push" part of the mechanism is performed by an electron-rich proximal imidazolate-like histidine fifth ligand.[8,10,23] The distal Arg38 residue likely aligns H_2O_2 in the active site and contributes to polarization of the O−O bond, also a "pull effect".[4] A similar active site environment exists in C*c*P.[9] "Push−pull" effects have been also implicated in O−O heterolysis leading to Cpd I formation in catalases and cytochromes P450.[1,2,9] Here a proximal tyrosinate likely provides the "push" for O−O heterolysis in catalase, while a distal histidine again "pulls".[24] It is proposed that cytochrome P450 enzymes compensate for the lack of acid−base "pull" residues in the distal cavity with a "strong push" from an electron-rich proximal cysteinate.[8,22,25−27]

Investigations of "push−pull effects" on Cpd I formation have been performed using heme model systems[10,17,28−31] and re-engineered myoglobin.[17−19,32] O−O heterolysis in acylperoxo porphyrin complexes is enhanced when electron-rich axial ligands are introduced or electron-releasing groups are attached to the *meso*-positions of the metalloporphyrin ring, simulating the "push".[10,28] "Pull effects" have been *indirectly* simulated in model complexes by using substituted peroxybenzoic acids.[10,29,30] Selective mutations in the distal cavity of myoglobin mutants have demonstrated the importance of a precisely positioned histidine as a proton shuttle—an H^+ "pull" residue—to the redox selectivity of peroxide O−O bond activation.[17−19,32]

The advantage of re-engineered proteins, as opposed to typical model systems, is that the H^+ pull residue is structurally established by the secondary and tertiary structure of the protein environment. Conversely, the secondary coordination environment of model compounds is difficult to control. Because H^+ residues are not oriented, "pull" effects cannot be systematically investigated. It is on this count that "Hangman" metallo-active sites are distinguished from typical model compounds. The Hangman architecture suspends an acid−base functional group over the face of redox-active macrocycles.[33−36] Crystal structures of the ferric Hangman complex containing a xanthene pillar and a pendent carboxylic acid $(HPX-CO_2H)Fe^{III}(OH)$ show that a structured water molecule is oriented between the distal acid group and hydroxide ligand of the heme via hydrogen bonding interactions.[33] The water molecule remains bound in solution, and titrations with base and H_2O have shown this binding to be chemically reversible. In this regard, the Hangman heme porphyrin is as a minimalist model for the secondary coordination environment of heme hydroperoxidase enzymes.[37,38] The hanging acid group mimics the amino acid residues that orient water in the distal cavities of heme peroxidases.

The precise positioning of the acid/base residue in Hangman complexes allows for the functional modeling of enzymatic "push−pull effects." $(HPX-CO_2H)Fe^{III}Cl$ exhibits exceptional catalytic activity upon peroxide activation for the catalase-like disproportionation of H_2O_2 and the cytochrome P450-like oxygenation of substrates.[33−38] It has been proposed that the hanging acid group facilitates O−O bond heterolysis to generate a Cpd I oxidant by shuttling H^+, similar to histidine "pull" residues in the active sites of peroxidase and catalase enzymes. Reported here are mechanistic experiments designed to probe *directly* the effects of a positioned acid group on internal redox partitioning in peroxide O−O bond activation to form Hangman Cpd I and II active sites.

Results

The reactions of ferric Hangman porphyrin complexes with peroxides were examined by stopped-flow techniques at cryogenic temperatures. In all cases, reactions were performed with Hangman metalloporphyrin complexes $(HPX-CO_2R$; R = Me, H) and the parent tetramesitylporphyrin (TMP) analogue for side-by-side comparison. This allowed for direct examination of the effects of a positioned acid−base group by providing a benchmark for comparative reactivity to the TMP system, which

(21) Poulos, T. L. In *Advances in Inorganic Biochemistry*; Eichhorn, G. L., Marzilli, L. G., Eds.; Elsevier: New York, 1988; Vol. 7, pp 1−36.
(22) Dawson, J. H. *Science* **1988**, *240*, 433−439.
(23) Heering, H. A.; Indiani, C.; Regelsberger, G.; Jakopitsch, C.; Obinger, C.; Smulevich, G. *Biochemistry* **2002**, *41*, 9237−9247.
(24) Fita, I.; Rossmann, M. G. *J. Mol. Biol.* **1985**, *185*, 21−37.
(25) Green, M. T.; Dawson, J. H.; Gray, H. B. *Science* **2004**, *304*, 1653−1656.
(26) Green, M. T. *J. Am. Chem. Soc.* **2006**, *128*, 1902−1906.
(27) Behan, R. K.; Green, M. T. *J. Biol. Inorg. Chem.* **2006**, *100*, 448−459.
(28) Groves, J. T.; Watanabe, Y. *J. Am. Chem. Soc.* **1988**, *110*, 8443−8452.
(29) Yamaguchi, K.; Watanabe, Y.; Morishima, I. *J. Am. Chem. Soc.* **1993**, *115*, 4058−4065.
(30) Traylor, T. G.; Ciccone, J. P. *J. Am. Chem. Soc.* **1989**, *111*, 8413−8420.
(31) Nam, W.; Lim, M. H.; Oh, S.-Y. *Inorg. Chem.* **2000**, *39*, 5572−5575.
(32) Watanabe, Y.; Ueno, T. *Bull. Chem. Soc. Jpn.* **2003**, *76*, 1309−1322.
(33) Yeh, C.-Y.; Chang, C. J.; Nocera, D. G. *J. Am. Chem. Soc.* **2001**, *123*, 1513−1514.
(34) Chang, C. J.; Yeh, C.-Y.; Nocera, D. G. *J. Org. Chem.* **2002**, *67*, 1403−1406.
(35) Liu, S.-Y.; Nocera, D. G. *J. Am. Chem. Soc.* **2005**, *127*, 5278−5279.
(36) Liu, S.-Y.; Soper, J. D.; Yang, J. Y.; Rybak-Akimova, E. V.; Nocera, D. G. *Inorg. Chem.* **2006**, *45*, 7572−7574.
(37) Chang, C. J.; Chng, L. L.; Nocera, D. G. *J. Am. Chem. Soc.* **2003**, *125*, 1866−1876.
(38) Chng, L. L.; Chang, C. J.; Nocera, D. G. *Org. Lett.* **2003**, *5*, 2421−2424.

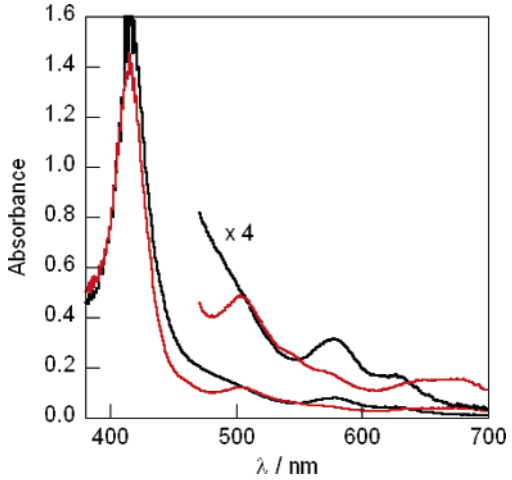

Figure 1. Stopped-flow UV−vis spectra from reaction of *m*-CPBA (3.5×10^{-4} M) with (HPX−CO_2Me)Fe^{III}(OH) (9.0×10^{-6} M) in CH_2Cl_2 at −40 °C to generate (HPX−CO_2Me)Fe^{III}(O_2COAr) at 0.1 s (black) and 50.0 s (red).

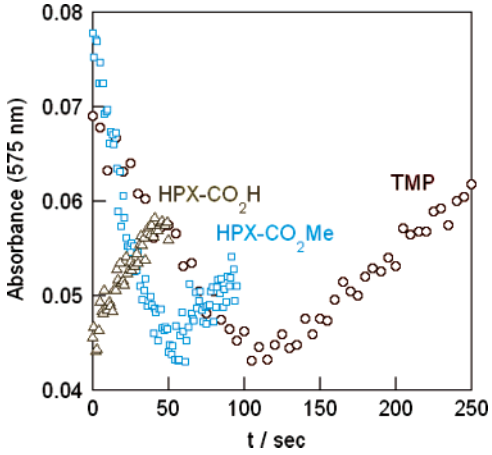

Figure 2. Selected time-resolved data for the disappearance of (P)Fe^{III}-(OH) (9.0×10^{-6} M; λ_{max} = 575 nm) in reactions with 3.5×10^{-4} M *m*-CPBA at −40 °C in CH_2Cl_2 to make (P)Fe^{III}(O_2COAr) and subsequent O−O bond heterolysis [P = TMP (○), HPX−CO_2Me (□), HPX−CO_2H (△)].

comprises an extensive literature for reactions of peroxides and peroxyacids with (TMP)Fe^{III}(OH).[10,28,29,31,39,40]

(HPX)Fe^{III} Substitution Chemistry. On mixing dichloromethane or toluene solutions of 3-chloroperoxybenzoic acid (*m*-CPBA) and (P)Fe^{III}(OH) at −40 °C (P = TMP, HPX−CO_2H, HPX−CO_2Me), a decrease is observed in the UV−vis absorption intensity of the 580 nm band of (P)Fe^{III}(OH) with a concomitant appearance of a Soret absorption band at 416 nm and a Q-band at 506 nm (Figures 1, S1). These new features are identical to previously reported spectra for the ferric acylperoxo complex (P)Fe^{III}(O_2COAr) (eq 1) that is generated from low-temperature substitution of hydroxide with 3-chloroperbenzoate when P = TMP.[28,29]

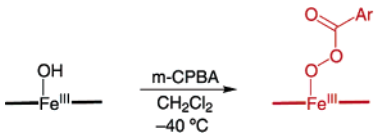

(1)

The similarity of these spectra indicates that analogous acylperoxo products are formed on the Hangman metalloporphyrin complexes. However, contrary to previous reports, substitution to make (TMP)Fe^{III}(O_2COAr) is not instantaneous.[28] Complete reaction requires >115 s in CH_2Cl_2 (at [(TMP)-Fe^{III}(OH)] = 9.0×10^{-6} M and [*m*-CPBA] = 3.4×10^{-5} M) at −40 °C.

Rigorous exclusion of ambient light is essential for reproducibility. The formation of (P)Fe^{III}(O_2COAr) is accelerated with increased [*m*-CPBA] or with exposure to light in CH_2Cl_2, presumably due to the in situ formation of trace HCl.[41] Similar axial substitution to form a Hangman analogue (HPX−CO_2Me)Fe^{III}(O_2COAr) is faster (~60 s), whereas formation of (HPX−CO_2H)Fe^{III}(O_2COAr) is complete in <10 s under identical reaction conditions (Figure 2). In sum, these results indicate an acid-assisted substitution reaction. More importantly, the trend in substitution HPX−CO_2H > HPX−CO_2Me > TMP suggests that the protonic microenvironment about the active site in Hangman metalloporphyrins is positioned to participate in reactions at the ferric heme center.

O−O Bond Heterolysis. In CH_2Cl_2 solutions, formation of (P)Fe^{III}(O_2COAr) complexes at −40 °C is immediately followed by a second set of spectral changes that are characterized by a blue shift and decrease in the Soret band intensity (to 406 nm and $\epsilon \approx 70\,000$ M^{-1} cm^{-1}) and formation of tailing features between 600 and 700 nm (Figures 3 and 4). These exactly match the well-established spectra of iron(IV) oxoporphyrin cation radicals.[42,43] The observed changes can therefore be assigned to heterolytic scission of the O−O bond to furnish Cpd I (P$^{\bullet+}$)-Fe^{IV}=O (eq 2).

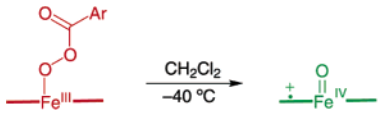

(2)

As illustrated in Figure 3b, the decay of the Soret band for (TMP)Fe^{III}(O_2COAr) at 416 nm occurs with concomitant growth of a Cpd I feature at 678 nm. Cpd I yields and rate constants for the heterolytic cleavage were obtained by global analysis of the full spectral window (380−700 nm). Both the growth and decay are simultaneously fit well by a first-order exponential equation with $k_{obsd} = (6.5 \pm 1.0) \times 10^{-3}$ s^{-1} (at [*m*-CPBA] = 3.4×10^{-5} M), indicating that heterolytic cleavage to generate (TMP$^{\bullet+}$)Fe^{IV}=O occurs without intermediates. The observed rate constant concurs with a previously reported rate constant for the same reaction.[28]

In contrast to TMP Cpd I formation, the decrease in the intensity of the Soret band for the Hangman (HPX)Fe^{III}(O_2-COAr) complexes at 416 nm is not solely due to Cpd I formation, as indicated by the biphasic nature of the time-resolved intensity at 678 nm (Figure 4b). The full-spectral data are best fit by an $A \rightarrow B \rightarrow C$ kinetic model with two sequential exponential equations corresponding to two first-order processes. The spectral changes observed in the $A \rightarrow B$ phase are consistent

(39) Bruice, T. C. *Acc. Chem. Res.* **1991**, *24*, 243−249.
(40) Lee, W. A.; Yuan, L.-C.; Bruice, T. C. *J. Am. Chem. Soc.* **1988**, *110*, 4277−4283.
(41) Exposure of (TMP)Fe^{III}(OH) to ambient light in anhydrous CH_2Cl_2 gives quantitative conversion to (TMP)Fe^{III}Cl.
(42) Groves, J. T.; Haushalter, R. C.; Nakamura, M.; Nemo, T. E.; Evans, B. J. *J. Am. Chem. Soc.* **1981**, *103*, 2884−2886.
(43) Groves, J. T.; Han, Y. In *Cytochrome P-450 Structure, Mechanism and Biochemistry*; Ortiz de Montellano, P. R., Ed.; Plenum Press: New York, 1986; pp 3−48.

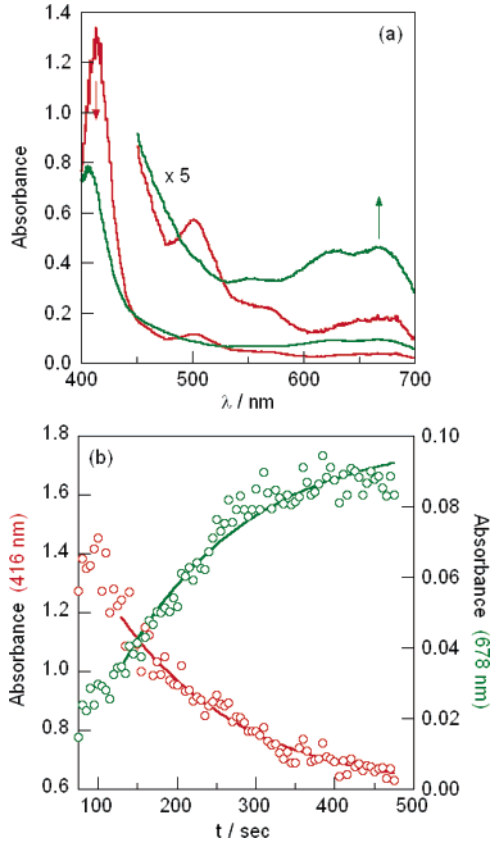

Figure 3. (a) Formation of Cpd I ($TMP^{\bullet+}$)Fe^{IV}═O (green line) from O—O heterolysis on 9.0×10^{-6} M (TMP)$Fe^{III}(O_2COAr)$ (red line) in CH_2Cl_2 at −40 °C. (b) Selected stopped-flow data for the disappearance of (TMP)-$Fe^{III}(O_2COAr)$ (red ○, $\lambda_{max} = 416$ nm) and concomitant appearance of Cpd I ($TMP^{\bullet+}$)Fe^{IV}═O (green ○, $\lambda_{max} = 678$) at [*m*-CPBA] $= 3.5 \times 10^{-5}$ M. Global data analysis gives $k_{obsd} = (6.5 \pm 1.0) \times 10^{-3}$ s^{-1}.

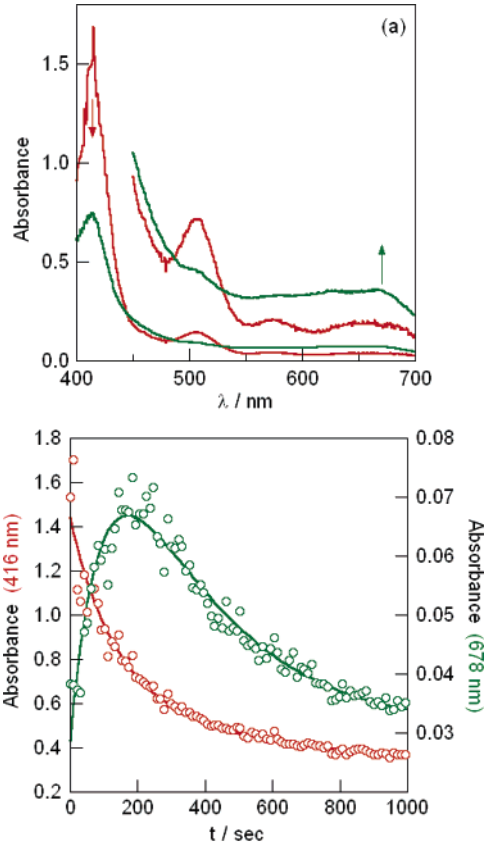

Figure 4. (a) Formation of Cpd I ($HP^{\bullet+}X—CO_2H$)Fe^{IV}═O (green line) from O—O heterolysis on 9.0×10^{-6} M ($HPX—CO_2H$)$Fe^{III}(O_2COAr)$ (red line) in CH_2Cl_2 at −40 °C. (b) Selected stopped-flow data for the disappearance of (TMP)$Fe^{III}(O_2COAr)$ (red ○, $\lambda_{max} = 416$ nm) and concomitant appearance of Cpd I ($TMP^{\bullet+}$)Fe^{IV}═O (green ○, $\lambda_{max} = 678$) at [*m*-CPBA] $= 1.0 \times 10^{-4}$ M. The biphasic data are best fit globally with two sequential exponential equations where $k_1 = k_{heterolysis} = (1.0 \pm 0.2) \times 10^{-2}$ s^{-1}.

with heterolytic O—O bond cleavage to generate Cpd I ($HP^{\bullet+}X$)-Fe^{IV}═O transients, while the $B \rightarrow C$ phase of the reaction occurs with a full-spectrum bleach of the Cpd I species. The sequential nature of the spectral evolution suggests that the decomposition originates from the high-valent Cpd I intermediate and occurs at a rate comparable to that for O—O bond heterolysis. Both heterolysis and subsequent decomposition are accelerated by increased [*m*-CPBA] (Table S1). Perhaps surprisingly, the rates of Cpd I formation are not significantly perturbed by the substitution of an ester for the acid functional groups on the Hangman scaffold, with $k_{obsd} = (1.0 \pm 0.3) \times 10^{-2}$ s^{-1} for $HPX—CO_2Me$ and $k_{obsd} = (6 \pm 3) \times 10^{-3}$ s^{-1} for $HPX—CO_2H$ at [*m*-CPBA] $= 3.4 \times 10^{-5}$ M.

O—O Bond Homolysis. In toluene, generation of (TMP)-$Fe^{III}(O_2COAr)$ at −20 °C is immediately followed by the formation of a new species with a red-shifted Soret band at 441 nm (Figure 5a) that is identical to the previously reported spectrum of a ferric porphyrin *N*-oxide complex.[28,43] Formation of the ferric porphyrin *N*-oxide product apparently results from an O—O bond homolysis process where the initially formed Cpd II (TMP)Fe^{IV}═O is rapidly consumed in a subsequent reaction with excess *m*-CPBA.[28] However, under the same reaction conditions ([Fe^{III}] $= 9.0 \times 10^{-6}$ M and [*m*-CPBA] $= 2.7 \times 10^{-5}$ M), with P = $HPX—CO_2Me$ the ferric *N*-oxide is formed in only 24% relative yield (Figure S2); no ferric *N*-oxide product is observed in reactions when P = $HPX—CO_2H$ (Figure 6). These results indicate that porphyrin *N*-oxide formation (an indirect measure of homolysis and Cpd II yield)[28] is significantly depressed by the Hangman scaffold. For this reason, the *N*-oxide spectrum is most easily observed for TMP (Figure 5) as opposed to Hangman platforms (Figure S2 for $HPX—CO_2Me$ and no spectral change on time scale shown in Figure 6 for $HPX—CO_2H$).

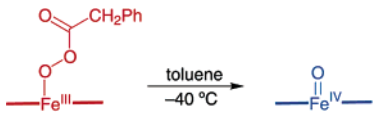

(3)

A more direct measure of Cpd II yield is obtained from reactions of (P)Fe^{III}(OH) with 1.2 equiv of phenylperoxyacetic acid (PPAA) at −40 °C ([Fe^{III}] $= 9.0 \times 10^{-6}$ M and [PPAA] $= 1.1 \times 10^{-5}$ M). Hydroxide exchange by peracetate to make (P)$Fe^{III}(O_2COCH_2Ph)$ is complete in seconds. When P = TMP or $HPX—CO_2Me$, the substitution is immediately followed by the formation of a new compound with a Soret band at 416 nm and a Q-band at 540 nm that match exactly the

(44) Cheng, R.; Latos-Grazynski, L.; Balch, A. L. *Inorg. Chem.* **1982**, *21*, 2412−2418.
(45) Calderwood, T. S.; Bruice, T. C. *Inorg. Chem.* **1985**, *25*, 3722−3724.

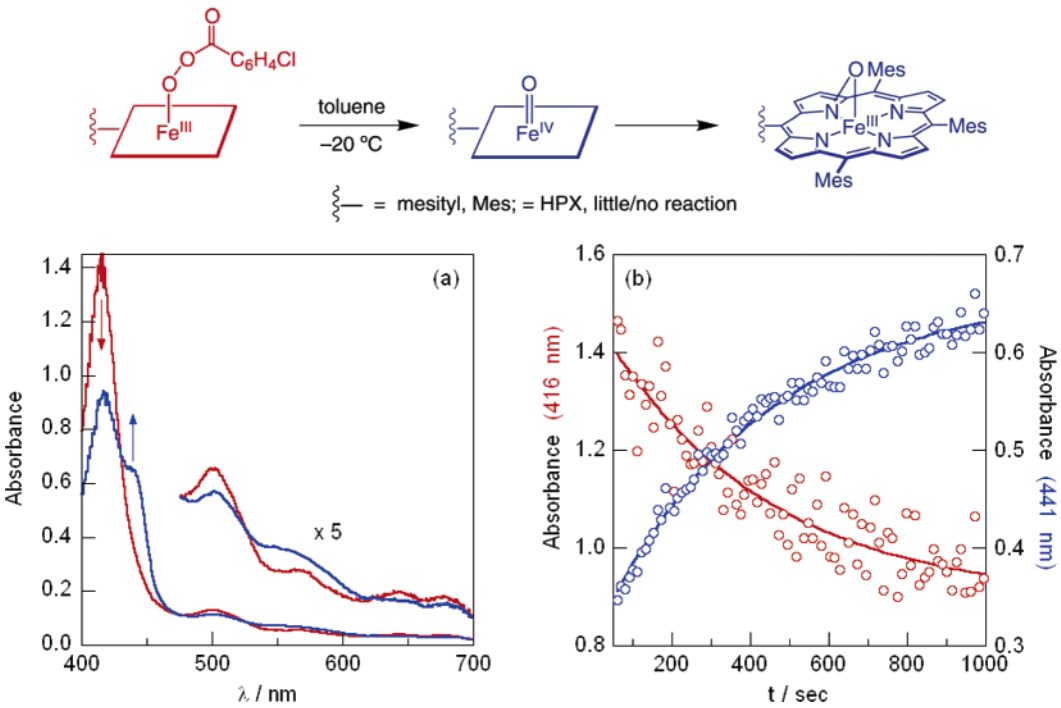

Figure 5. (a) Stopped-flow UV−vis spectra from reaction of *m*-CPBA (2.7×10^{-5} M) with (TMP)Fe^{III}(OH) (9.0×10^{-6} M) (red line) in toluene at −20 °C to generate a ferric *N*-oxide, homolysis product (blue line). (b) Selected data for the disappearance of (TMP)Fe^{III}(OH) (red ○, λ_{max} = 416 nm) and simultaneous appearance of the *N*-oxide product (blue ○, λ_{max} = 441 nm). As indicated in heading, formation of the *N*-oxide is greatly suppressed when mesityl is replaced by a Hangman scaffold.

bands in the well-known spectrum of Cpd II (P)Fe^{IV}=O, the product of O−O bond homolysis (eq 3).[28,29,44,45]

Full-spectral fitting indicates the Cpd II material is generated in ∼70% yield at 60 s, and isosbestic features at 523 and 560 nm indicate that O−O homolysis occurs without the intervention of intermediates on the time scale of the stopped-flow experiment (Figure 7). Treatment of the acid Hangman complex (HPX−CO_2H)Fe^{III}(OH) with PPAA shows only a very slow full-spectral bleach. No Cpd II homolysis products are observed. This is not due to an inherent instability of the homolysis product, as Cpd II (HPX−CO_2H)Fe^{IV}=O has been previously generated under different reaction conditions.[37] In sum, these results suggest that the acid−base residue of the Hangman system is preventing Cpd II formation by inhibition of $1e^-$ homolytic O−O bond activation.

Discussion

Analysis of cryogenic stopped-flow reactions of (P)Fe^{III}(OH) with peroxyacids in aprotic solvents shows the influence of an intramolecular proton donor on reactions at the ferric porphyrin center in Hangman metalloporphyrin complexes. The acid−base group is manifest in two ways: (1) Acid-assisted axial ligand substitution of hydroxide to form the ferric acylperoxo products (P)Fe^{III}(O_2COAr) is accelerated by the acidic environment proximate to the iron center in the HPX−CO_2H complex; (2) the stopped-flow studies demonstrate the ability of the acidic "pull" functionality to effect selective redox chemistry on the heme iron in subsequent O−O bond activation of peroxide.

As summarized in Scheme 2, the effects of a properly oriented H^+-directing group favor heterolytic ($2e^-$) O−O bond cleavage over competing homolysis ($1e^-$) pathways. This selectivity appears to have a kinetic basis. Reactions of all the (P)Fe^{III}(OH) materials with *m*-CPBA give exclusively the expected even-electron heterolysis Cpd I product, as shown in pathway *b*. However, generation of Cpd I in these conditions is not kinetically more facile for the (HPX−CO_2H)Fe^{III}(OH) reactant as compared to (P)Fe^{III}(OH) (P = TMP or HPX−CO_2Me). The pseudo first-order rate constants for O−O bond heterolysis of the bound peroxide are the same within error for all porphyrin macrocycles investigated here. In contrast, formation of Cpd II products by a single-electron homolysis reaction, pathway *c*, is strongly affected by a proximal H^+ donor. Under conditions that are known to favor peroxide O−O bond homolysis, generation of Cpd II products is strongly disfavored in Hangman metalloporphyrin systems vs the parent TMP complex. No O−O homolysis products are observed in reaction with *m*-CPBA or PPAA in toluene when P = HPX−CO_2H. While the ultimate fate of the Hangman products in these reactions has not been established, the presence of an H^+ donor pendent group clearly introduces a kinetic barrier to the odd-electron reaction pathway.

In this context, the high catalytic efficiencies of Hangman metalloporphyrins as measured by increased TON relative to the parent TMP analogues in mono-oxygenase and catalase-type reactions merit evaluation.[37,38] Three factors may rationalize this superior activity of Hangman porphyrin systems: (A) A properly positioned Hangman carboxylic acid residue may increase the rate of O−O heterolysis and Cpd I formation in a rate-determining peroxide activation. (B) The Hangman porphyrin catalyst is inherently more stabile toward destructive self-oxidation by the high-valent ($P^{\bullet+}$)Fe^{IV}=O transients and increased catalyst lifetime leads to increased TON. (C) The Hangman architecture impacts the ratio of productive heterolytic O−O activation to homolytic O−O scission that generates (P)-Fe^{IV}=O materials. In scenario C, the Cpd II products are poor

Scheme 2[a]

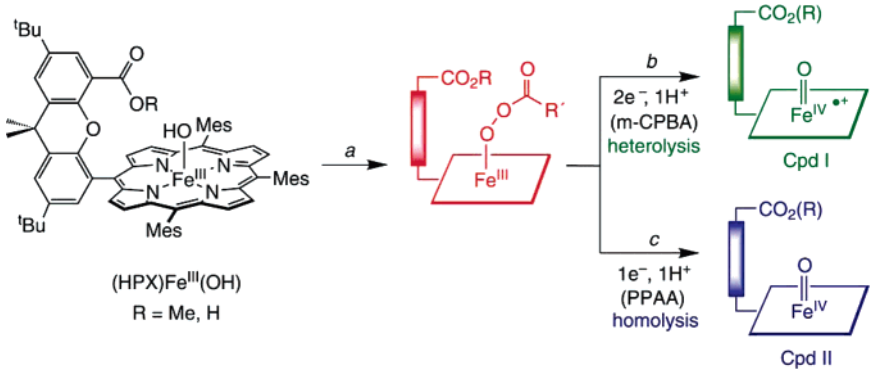

(a) HO_2COR' [R' = CH_2Ph (PPAA), C_6H_4Cl (m-CPBA)], CH_2Cl_2 or toluene, −40 °C. (b) R' = C_6H_4Cl, CH_2Cl_2, −40 °C. (c) R' = CH_2Ph, toluene, −40 °C.

Scheme 3

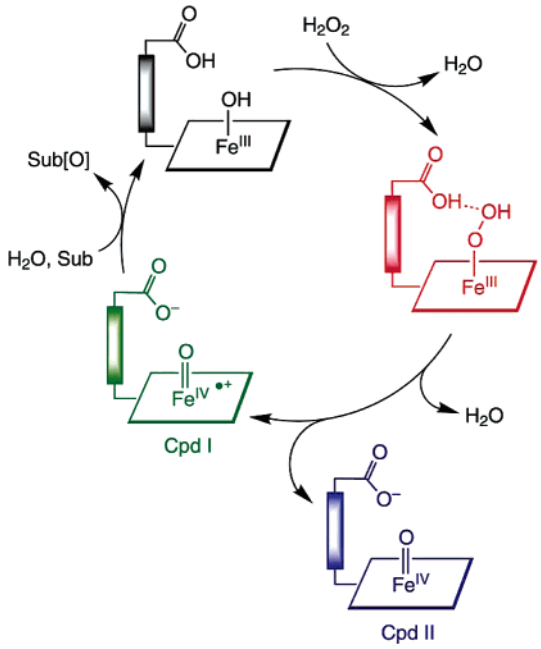

oxidants and are outside the catalytic cycle. The stopped-flow kinetics results described here strongly support scenario C over A and B and accordingly lead to the cycle shown in Scheme 3 where Cpd II formation represents a catalyst deactivation pathway. The stopped-flow experiments establish that O—O heterolysis of the peroxide, and Cpd I formation is not accelerated by the acid−base hanging group, disfavoring A. The Hangman system is in fact less stable toward decomposition under the reaction conditions, suggesting that B is unlikely. However, the stopped-flow studies do show that the positioned acid group in HPX−CO_2H disfavors a homolytic O—O cleavage pathway and Cpd II formation. This implies that redox selectivity in O—O bond activation is in fact more important that the stability of the catalyst itself. By removing a competing pathway for O—O bond activation, the Hangman catalysts maintain a lower concentration of catalytically inactive Cpd II oxidant. The HPX−CO_2H complex thus exhibits high turnover numbers and consequently is a more efficient catalyst, despite its proclivity toward self-oxidation.

Proton-directed redox specificity for multielectron reactivity of the Hangman metalloporphyrins nicely complements the experiments of Watanabe and co-workers where mutations to

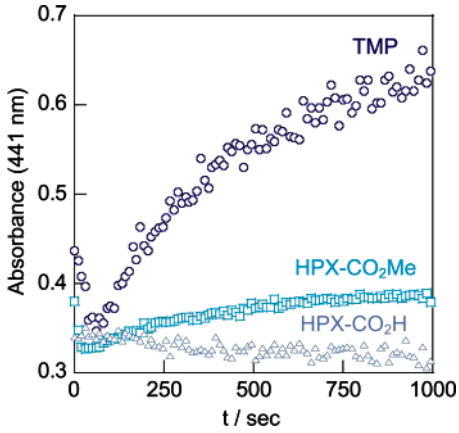

Figure 6. Formation of ferric *N*-oxide products (with λ_{max} = 441 nm) for P = TMP (○), HPX−CO_2Me (□), and HPX−CO_2H (△) at [Fe^{III}] = 9.0 × 10^{-6} M and [*m*-CPBA] = 2.7 × 10^{-5} M at −20 °C in toluene.

re-engineer myoglobin perturb the ratios of heterolytic to homolytic O−O bond cleavage in peroxide activation.[17,19,32] Their work suggests that precise positioning of a distal histidine residue near the iron active site is essential for enzymatic O−O heterolysis to make a peroxidase-like Cpd I species. Similarly, we show here that the positioned acidic functional group near a ferric heme center effects redox partitioning in O−O bond activation by favoring a proton-coupled $2e^-$ reaction over a competing $1e^-$ pathway. The demonstration of such proton-directed $2e^-$ vs $1e^-$ redox control in a small-molecule model system is key to future advances in the basic science of multielectron redox chemistry, and especially reactivity pertaining to O−O bond formation and breaking reactions. To this end, the work has consequence to bioenergy conversion schemes[46−51] and points the way to the design of O−O bond breaking mimics (cytochrome c oxidase) and O−O bond making mimics (artificial photosynthetic systems).

(46) Dempsey, J. L.; Esswein, A. J.; Manke, D. R.; Rosenthal, J.; Soper, J. D.; Nocera, D. G. *Inorg. Chem.* **2005**, *44*, 6879−6892.
(47) Eisenberg, R.; Nocera, D. G. *Inorg. Chem.* **2005**, *44*, 6799−6801.
(48) Chang, C. J.; Chang, M. C. Y.; Damrauer, N. H.; Nocera, D. G. *Biophys. Biochim. Acta* **2004**, *1655*, 13−28.
(49) Reece, S. Y.; Hodgkiss, J. M.; Stubbe, J.; Nocera, D. G. *Philos. Trans. R. Soc. London, Ser. B* **2006**, *361*, 1351−1364.
(50) Lewis, N. S.; Nocera, D. G. *Proc. Natl. Acad. Sci. U.S.A.* **2006**, *103*, 15729−15735.
(51) Nocera, D. G. *Dædalus* **2006**, *135*, 112−115.
(52) Kadish, K. M; Smith, K. M.; Guilard, R. *The Porphyrin Handbook*; Academic Press: San Diego, CA, 2000; and references therein.
(53) Silbert, L. S.; Siegel, E.; Swern, D. *J. Org. Chem.* **1962**, *27*, 1336−1342.

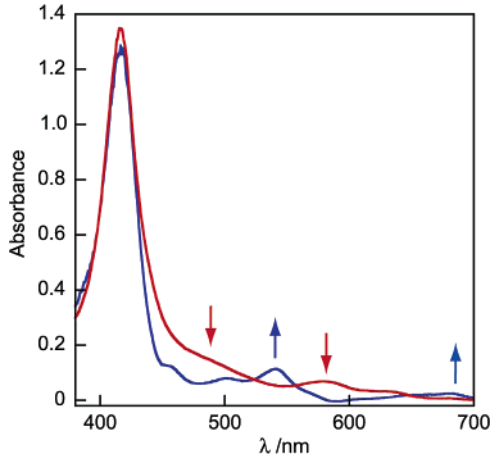

Figure 7. UV−vis spectra of (TMP)$Fe^{III}(O_2COCH_2Ph)$ (red line) and Cpd II (TMP)Fe^{IV}═O (blue line) obtained from global analysis (350−700 nm) of a stopped-flow reaction of 9.0×10^{-6} M (TMP)Fe^{III}(OH) with 1.1×10^{-5} M PPAA in toluene at −40 °C. No Cpd II homolysis products are observed for (HPX−CO_2H)Fe^{III}(OH).

Experimental Details

General Considerations. All manipulations were performed under an inert atmosphere, in nitrogen- or argon-filled glove boxes or using standard Schlenk techniques, unless otherwise noted. Routine UV−vis spectra were obtained with a Spectral Instruments SI400 Series diode array spectrophotometer (350 to 700 nm) at ambient temperature. Kinetics measurements were made using a Hi-Tech Scientific SF-43 multimixing anaerobic cryogenic stopped-flow instrument equipped with a Hi-Tech Scientific Kinetascan diode array rapid scanning unit. Full-spectral kinetics data were fit globally with the commercially available software Specfit32 from Spectrum Software Associates or at single wavelengths or with IS-2 Rapid Scanning Kinetic Software (Hi-Tech Scientific). In all kinetic global analyses, rate constants were obtained by fitting to an appropriate kinetic model and minimization without constraints. Multiple starting points for the iterations were chosen to ensure that minima were not localized. Global fits were evaluated by rms deviations and comparison of calculated spectra with experimental data.

Materials. Solvents were purchased from VWR Scientific Products, passed through an M. Braun purification system and sparged with N_2 to remove trace O_2 prior to use. The porphyrin compounds (TMP)-Fe^{III}(OH),[52] (HPX−CO_2H)Fe^{III}(OH),[37] and (HPX−CO_2Me)Fe^{III}(OH)[37] were prepared according to published methods. 3-Chloroperoxybenzoic acid (*m*-CPBA) was purchased from Aldrich (77%) and purified by washing with pH 7.40 phosphate buffer and recrystallization from pentane to remove 3-chlorobenzoic acid. Purity (>95%) was determined by ^{1}H NMR.

Phenylperoxyacetic acid (PPAA) was prepared by adapting a literature procedure.[53] Dropwise addition of 50% H_2O_2 (3.0 mL, 90 mmol) to a vigorously stirring solution of 0.31 M phenylacetic acid (4.08 g, 30 mmol) in methanesulfonic acid (9.7 mL, 150 mmol) gave a white precipitate. The temperature was maintained below 28 °C in a water bath during H_2O_2 addition and then heated to 30 °C for 40 min. The slurry was cooled to 10 °C, and ∼15 mg of ice were added. The solids were collected by filtration and washed with 40 mL of ice-cold water to obtain phenylperoxyacetic acid (PPAA) (4.18 g, 91%). The crude material was purified by washing with phosphate buffer and recrystallized from pentane to remove residual acid. Purity (>95%) was checked by ^{1}H NMR.

Stopped-Flow Kinetics. In a representative procedure, a gastight syringe was charged with 1.8×10^{-5} M (TMP)Fe^{III}(OH) in toluene (25 mL, 0.45 μmol). A second gastight syringe was charged with 7.0×10^{-5} M *m*-CPBA in toluene (25 mL, 1.75 μmol). Precautions were taken to exclude ambient light rigorously. The solutions were loaded into the stopped-flow spectrophotometer and triggered by simultaneous injection of 0.1 mL of each solution to make the reactant concentrations 9.0×10^{-6} M and 3.5×10^{-5} M in iron and *m*-CPBA, respectively. The solutions were cooled to −40 °C prior to mixing and maintained at that temperature in a chilled heptane bath throughout the reaction. The reaction was monitored by UV−vis spectroscopy. Spectra (350−700 nm) were acquired for 100 s at 0.5 s intervals. Data were analyzed as described in Results and Discussion.

Acknowledgment. Financial support for this research was provided by the National Institutes of Health (GM 47274) and the U.S. Department of Energy (DOE DE-FG02-05ER15745 (DGN) and NSF CHE-0111202 (EVRA). J.D.S. gratefully acknowledges support from an NIH Ruth L. Kirschstein postdoctoral fellowship (GM 69244).

Supporting Information Available: Table S1 and Figures S1 and S2. This material is available free of charge via the Internet at http://pubs.acs.org

JA0683032